Theoretical analysis of defect-mediated turbulence in a catalytic surface reaction

Dagmar Krefting[1] and Carsten Beta[2]
[1]*Charité–Universitätsmedizin Berlin, Campus Benjamin Franklin (CBF), Hindenburgdamm 30, 12200 Berlin, Germany*
[2]*Institut für Physik und Astronomie, Universität Potsdam, Karl-Liebknecht-Strasse 24/25, 14476 Potsdam-Golm, Germany*
(Received 2 April 2009; revised manuscript received 6 January 2010; published 8 March 2010)

We present a statistical analysis of defect-mediated turbulence in a kinetic model of catalytic CO oxidation on Pt(110). A probabilistic description based on the gain and loss rates of defects is derived. For low values of the CO partial pressure the statistics of topological defects agree with earlier results for the complex Ginzburg-Landau equation. For high values of the CO partial pressure, we observe an additional autocatalytic reproduction of defects that results in a linear dependence of the defect creation rate on the number of defects in the system. The role of correlations between defects of opposite topological charge was found to be weaker than in the experimental system.

DOI: 10.1103/PhysRevE.81.036209 PACS number(s): 05.45.−a, 82.40.Np, 82.40.Qt

I. INTRODUCTION

The emergence of spatiotemporal structures in nonequilibrium systems has been intensively investigated over the past decades [1,2]. Research in this interdisciplinary field ranges from fundamental physics to chemical applications and complex living systems [3]. Besides ordered patterns, also irregular chaotic behavior can be observed in such systems. While deterministic chaos in low-dimensional dynamical systems is well understood (see, e.g., Ref. [4] and other standard text books), disorder in high-dimensional, spatially extended systems remains one of the outstanding open problems in this field.

In many extended pattern forming systems, disordered states are characterized by the emergence of amplitude defects. Such states are generally referred to as defect-mediated turbulence [5]. A statistical description of defect dynamics has been established as a unifying approach to characterize spatiotemporal disorder in these systems. Defect dynamics has been analyzed in generic model systems, such as the complex Ginzburg-Landau equation (CGLE) [5–7] and the FitzHugh-Nagumo system [8]. Also, defect statistics in the presence of noise [9,10] and for systems with chaotic local dynamics has been considered [11]. Recently, the theoretical study of defect dynamics was extended to three-dimensional excitable media, where the end points of scroll wave filaments on the border of the medium constitute topological defects with statistical properties that are clearly distinct from a purely two-dimensional system [12]. The first probabilistic description of defect mediated turbulence was developed by Gil *et al.* for the CGLE [6]. They consider topological defects as statistically independent entities that are created and annihilated in pairs of opposite topological charge. In their model, defect creation is a random event that does not depend on the number of defect pairs n in the system and is only determined by the choice of the system parameters. Defect annihilation, on the other hand, requires that two defects of opposite charge meet, i.e., will occur proportional to n^2. Based on the corresponding gain and loss rates k_+ and k_-, they derived a squared Poisson distribution for the number of defects in the system that shows good agreement with the distribution found in numerical simulations of the CGLE.

Laboratory observations of defect turbulence have been reported from a number of nonlinear experimental systems, namely, electroconvection in liquid crystals [13], fluid convection [14,15], electrochemical systems [16], and the Belousov-Zhabotinsky (BZ) reaction [17]. Besides the BZ reaction, the catalytic oxidation of CO on Pt(110) has been established as a paradigmatic experimental model system to study spatiotemporal pattern formation in a chemical reaction-diffusion system far from thermodynamic equilibrium [18]. Compared to other heterogeneous catalytic surface chemical reactions, catalytic CO oxidation on Pt(110) exhibits exceptionally rich spatiotemporal dynamics [19]. The CO oxidation system has been used in numerous studies of spatiotemporal pattern formation, including control of chaos [20–22] and engineering of self-organized structures by periodic forcing [23,24], global feedback [25,26], and localized heterogeneities [27,28].

Spatiotemporally chaotic states have already been reported together with the first observations of pattern formation in catalytic CO oxidation [29]. In the context of chemical systems, they are typically referred to as chemical turbulence. Recently, the first statistical analysis of defect-mediated turbulence in experiments of catalytic CO oxidation has been presented [30]. In contrast to the findings of Gil *et al.* for the CGLE, the experimental data showed a combined linear and quadratic dependence of the annihilation rate on n. In this case, the probability density function (PDF) takes the form of a modified Poisson distribution [15,30]. The additional linear contribution to the annihilation has been explained by the presence of strong short-range correlations between defects of opposite topological charge. Such correlations lead to an increased number of self-annihilation events, in which defects are annihilating with the same oppositely charged partner defect that they have been created with. In this case, the two defects cannot be treated as well-mixed objects. They are not statistically independent so that self-annihilation will scale linearly with n. In the present paper, we complement this experimental work with theoretical data obtained in the framework of a well-established kinetic model of catalytic CO oxidation, the Krischer-Eiswirth-Ertl (KEE) model [31]. Since the early 1990s, the KEE model has been successfully used to interpret the complex spatiotemporal behavior of catalytic CO

 ©2010 The American Physical Society

oxidation. In general, there is no quantitative agreement between the behavior of the experimental system and the KEE model. However, to a qualitative extent, all the dynamical features of catalytic CO oxidation are accounted for in the KEE model. Results on defect statistics have been reported for a periodically forced version of this model in the context of front explosion phenomena [32]. However, no analysis of defect turbulence is available for the unperturbed KEE system.

II. NUMERICAL MODEL AND METHODS

A. KEE model

The KEE model of catalytic CO oxidation on Pt(110) takes all the prominent features of this surface catalytic reaction into account, in particular, the adsorption of CO and oxygen, the desorption of CO, the reaction of adsorbed CO molecules and oxygen atoms, the surface diffusion of CO, and the adsorbate induced structural phase transition of the Pt(110) surface between the (1×1) bulk structure and the (1×2) missing row structure. A number of secondary properties such as surface faceting, the formation of subsurface oxygen, and global gas phase coupling are neglected in the original version of the KEE model.

Three dynamical variables characterize the state of the system, $u(\mathbf{r},t)$, $v(\mathbf{r},t)$, and $w(\mathbf{r},t)$ with $\mathbf{r}=(x,y)$. They describe the surface coverage with CO and O, and the local fraction of the surface in the nonreconstructed (1×1) phase, respectively. The time evolution of these fields is governed by the following system of equations,

$$\partial_t u = k_1 s_{\mathrm{CO}} p_{\mathrm{CO}}(1-u^3) - k_2 u - k_3 uv + D\nabla^2 u, \tag{1}$$

$$\partial_t v = k_4 p_{\mathrm{O}_2}[s_{\mathrm{O},1\times1} w + s_{\mathrm{O},1\times2}(1-w)](1-u-v)^2 - k_3 uv, \tag{2}$$

$$\partial_t w = k_5\left(\frac{1}{1+\exp[(u_0-u)/\delta u]} - w\right), \tag{3}$$

where k_1, k_2, and k_4 are the rate constants of CO adsorption, CO desorption, and oxygen adsorption, respectively. The parameters s_i with $i=(\mathrm{CO}),(\mathrm{O},1\times1),(\mathrm{O},1\times2)$ represent the sticking coefficients of CO and oxygen, the latter being different on the (1×1) and (1×2) surface structures. Furthermore, D is the coefficient of CO surface diffusion, k_3 denotes the rate constant of the reaction between adsorbed CO and oxygen, and k_5, u_0, δu control the surface structural transition between the (1×1) and (1×2) phases. The numerical values of all modeling parameters are summarized in Table I. The values of CO and oxygen partial pressures are chosen in the oscillatory regime where uniform oscillations are unstable and chemical turbulence spontaneously emerges. A snapshot of the CO coverage u from a turbulent time series can be seen in Fig. 1(a). For a systematic scan of the dynamics of the spatially extended KEE model see Ref. [33].

Numerical simulations are performed using a second-order finite difference scheme for the spatial discretization with a grid resolution of $dx=4$ μm. A system size of 400 $\times 400$ $\mu\mathrm{m}^2$ with periodic boundary conditions is chosen. For time integration, an explicit Euler scheme with a fixed time step of $dt=0.001$ s is used. Simulations are performed for different levels of CO pressure, each of them over a total simulation time of 1000 s. We systematically increase the CO partial pressure from 4.6×10^{-5} to 4.7×10^{-5} mbar in increments of 2×10^{-7} mbar. For the chosen oxygen partial pressure of $p_{\mathrm{O}_2}=12.0\times10^{-5}$ mbar, this interval spans almost the entire turbulent regime [33].

TABLE I. Parameters of the numerical model.

Parameter	Value	Description
k_1	3.14×10^5 s^{-1} mbar^{-1}	Impingement rate of CO
k_2	10.21 s^{-1}	CO desorption rate
k_3	283.8 s^{-1}	Reaction rate
k_4	5.86×10^5 s^{-1} mbar^{-1}	Impingement rate of O_2
k_5	1.610 s^{-1}	Phase transition rate
s_{CO}	1.0	CO sticking coefficient
$s_{\mathrm{O},1\times1}$	0.6	Oxygen sticking coefficient on the 1×1 phase
$s_{\mathrm{O},1\times2}$	0.4	Oxygen sticking coefficient on the 1×2 phase
u_0, δu	0.35, 0.05	Parameters for the structural phase transition
D	40 $\mu\mathrm{m}^2$ s^{-1}	CO diffusion coefficient
p_{O_2}	12.0×10^{-5} mbar	O_2 partial pressure

B. Data processing

In order to detect topological defects, we transform the simulation results into a representation in terms of phase and amplitude variables. This is achieved following the empirical method established in Refs. [34,35]. We define amplitude and phase in the projection plane of the two model variables u and w. Deviations from harmonic oscillations are compensated by introducing a reference orbit, defined as the limit cycle of oscillations in the (u,w)-plane in absence of diffusion $(D=0)$. As origin of the (u,w) plane, we choose the unstable steady state (u_0,w_0) at the center of the limit cycle. The reference values are determined in a separate numerical simulation for each set of parameters. The phase ϕ of any local system state (u,w) is then defined as $\phi=2\pi\tilde{T}/T_{\mathrm{ref}}$. Here, $\tilde{T}$ is the time needed to proceed from some arbitrarily chosen, fixed initial location on the reference orbit along the orbit to the point that is defined by the direction of (u,w). The reference time T_{ref} is the period of the reference orbit. The amplitude R is defined as $R=\rho/\rho_{\mathrm{ref}}$, where ρ is the distance of the point (u,w) from the origin (u_0,w_0) and ρ_{ref} the distance from the origin to the reference orbit at the same phase. For more details on this definition of phase and amplitude variables see Ref. [34].

In Fig. 1, a snapshot of the u-field from a turbulent time series is displayed along with the corresponding phase and amplitude fields. In this representation, topological defects can be identified. The location of a defect is characterized by

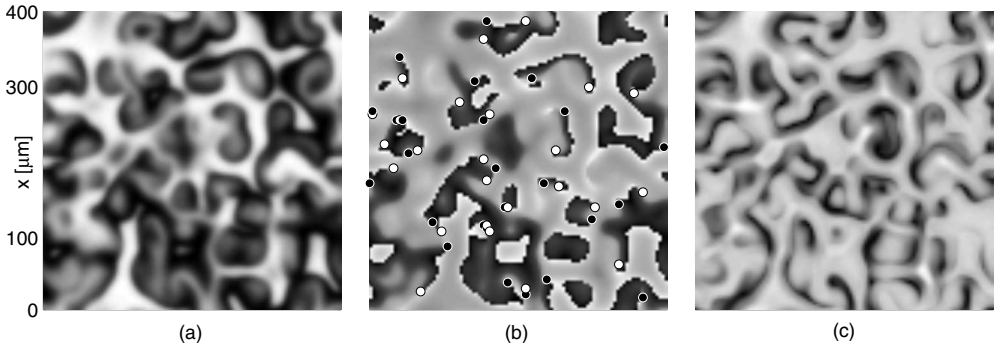

FIG. 1. Example of chemical turbulence in the KEE model. (a) CO coverage u, (b) phase, and (c) amplitude fields. Positive (negative) topological defects are indicated as open (filled) circles. The CO partial pressure is $p_{CO}=4.66\times10^{-5}$ mbar. The other parameters are as listed in Table I.

a vanishing amplitude. In the phase field, they coincide with the end points of isophase contour lines, where the phase is not defined and the phase gradient diverges. Such defects are characterized by an integer topological charge, i.e., around any closed contour surrounding a defect, the phase changes by an amount of $2\pi m_{top}$, with

$$m_{top}=\frac{1}{2\pi}\oint \nabla\phi(\mathbf{x},t)d\mathbf{s}. \tag{4}$$

The positions of defects are detected by identifying strong positive and negative extrema in the gradient field of the phase. In Fig. 1(b), topological defects have been marked according to their charge. Topological defects are created and annihilated in pairs of opposite topological charge so that the numbers of positively and negatively charged defects are equal in a system with periodic boundary conditions, $n_+=n_-\equiv n$. Defect detection is performed with a frame rate of 10 Hz, i.e., defect analysis is carried out for 10 000 frames of each simulation. The gain and loss rates are determined by polynomial fits of the numerical data. Here, the only processes that may change the number of defects are defect creation and annihilation. Border effects, i.e., entering and leaving due to defect mobility are absent because periodic boundary conditions are used in our simulations. Different forms of the probability distribution function (PDF) are determined and compared to the probability distribution of the defects obtained by the numerical simulations. For further evaluation of the statistical properties, also tracking of the individual defects is performed by using a next-neighbor particle tracking algorithm.

III. RESULTS

A. Numerical simulations

All simulations carried out within this study show fluctuating defect numbers in the course of time. Figure 2(a) shows exemplarily the time evolution of the number of defect pairs for $p_{CO}=4.60\times10^{-5}$ mbar and $p_{CO}=4.66\times10^{-5}$ mbar. The mean values are indicated by horizontal lines. In Fig. 2(b), the mean number of defect pairs is shown for the entire set of six simulations as a function of CO partial pressure. With increasing CO partial pressure, we first observe an increasing average number of defect pairs. At around $p_{CO}=4.65\times10^{-5}$ mbar, the number of defects becomes maximal and decreases when the CO partial pressure is increased further. The corresponding probability distributions have been determined for all cases, three of which are shown in Fig. 3.

Examples for both gain and loss rates are displayed in Fig. 4. They correspond to the three cases shown in Fig. 3. Both the squared and the modified Poisson distributions expect a constant creation rate, see black lines in Figs. 4(a)–4(c). They differ in an additional linear dependence of

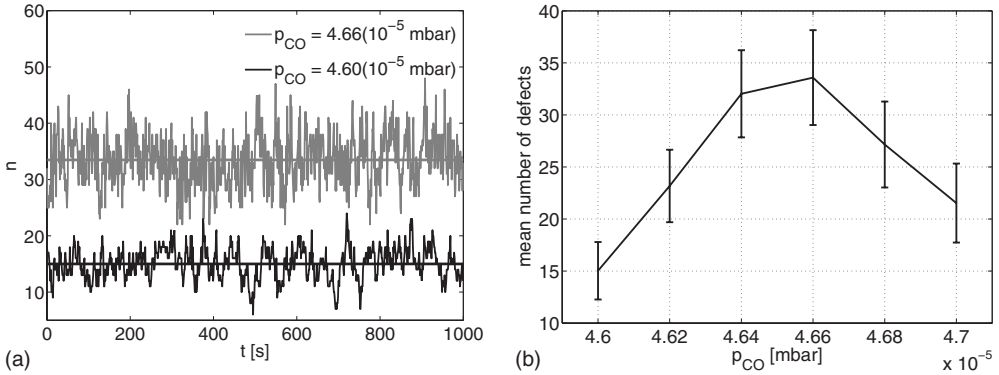

FIG. 2. (a) Number of defect pairs as a function of time for two different values of CO partial pressure, $p_{CO}=4.60\times10^{-5}$ mbar and $p_{CO}=4.66\times10^{-5}$ mbar. (b) Average number of defect pairs as a function of CO partial pressure.

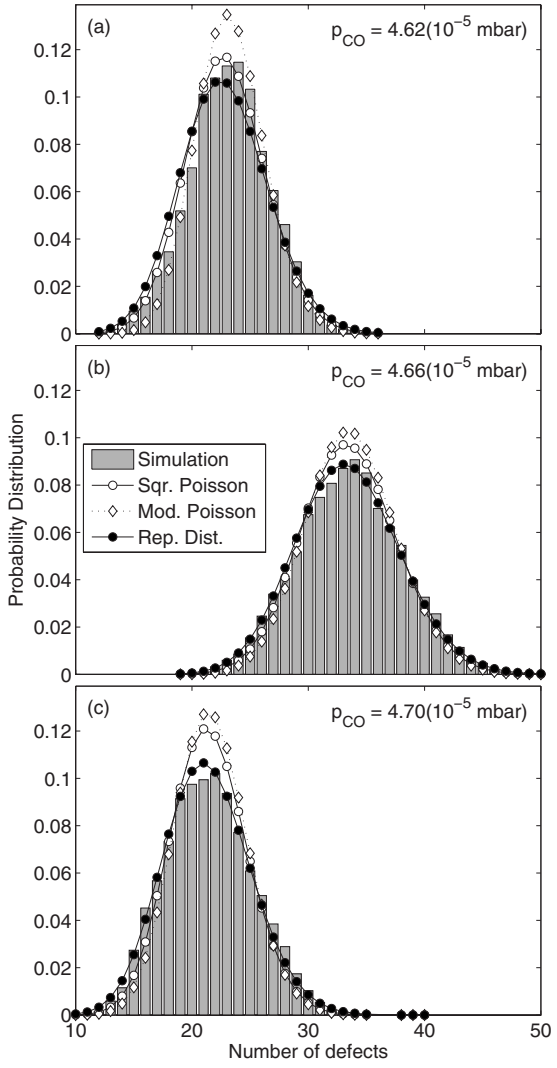

FIG. 3. Probability distributions obtained from the analysis of the numerical data (bars). The superposed curves show a squared Poisson distribution (open circles), a modified Poisson distribution (diamonds), and the replication distribution according to Eq. (9) (filled circles). The CO partial pressure is (a) $p_{CO}=4.62\times10^{-5}$ mbar, (b) 4.66×10^{-5} mbar, and (c) 4.70×10^{-5} mbar, respectively. The other model parameters are as listed in Table I.

the loss rate on n for the modified Poisson distribution. The annihilation rates found in the simulations of the KEE model are well approximated by a quadratic dependence on n, $k_-=an^2$, given as black lines in Figs. 4(d)–4(f). Only small improvements are found, when allowing for an additional linear term, see the gray lines in Figs. 4(d)–4(f). The resulting squared and modified Poisson distributions are depicted in Fig. 3. While the distribution at low CO partial pressure [Fig. 3(a)] is well described by the squared Poisson distribution, for higher CO partial pressures [Figs. 3(b) and 3(c)] the distribution is significantly broader than predicted by both the squared and the modified Poisson distribution. These deviations between numerical results and theoretical predictions are caused by a linear dependence of the defect creation rate on the number of defect pairs n, $k_+(n)=c+dn$. The value of d increases for larger CO partial pressures, i.e., the dependence of defect creation on the number of existing defects in the system becomes more pronounced. Therefore, we will derive a probability distribution function for the number of defect pairs taking this dependence into account.

B. Probabilistic model

Following Gil *et al.* [6], the master equation for the probability $p(n,t)$ of finding a number of n defects at time t in the system reads as

$$\partial_t p(n,t) = k_+(n-1)p(n-1,t) + k_-(n+1)p(n+1,t) - k_+(n)p(n,t) - k_-(n)p(n,t), \quad (5)$$

where $k_+(n)$ and $k_-(n)$ are the gain and loss rates of defects which may depend on the number of defects n. In the statistically stationary regime, $\partial_t p(n,t)=0$, Eq. (5) yields a simple recursive relation for the probability $p(n)$,

$$p(n) = \frac{k_+(n-1)}{k_-(n)} p(n-1). \quad (6)$$

To derive the probability distribution for the number of defects n, expressions for the gain and loss rates are required. Based on the results of the previous section, we take

$$k_+(n) = c + dn, \quad (7)$$

$$k_-(n) = an^2. \quad (8)$$

Inserting the expressions for k_+ and k_- into Eq. (6) the following probability distribution is obtained:

$$p(n) = Q\frac{\gamma^n \Gamma(\nu+n)}{(n!)^2}, \quad (9)$$

with $\gamma=\frac{d}{a}$ and $\nu=\frac{c}{d}$. The distribution [Eq. (9)] is termed the *replication distribution*. Normalization requires

$$Q = \frac{1}{\Phi(\nu,1;\gamma)\Gamma(\nu)}, \quad (10)$$

where Φ denotes the degenerate hypergeometric function. See the Appendix for details of the derivation of the replication distribution [Eq. (9)].

The values of a, c, and d are given by the fit parameters of the rate constants displayed in Fig. 4. The corresponding values of $\gamma=\frac{d}{a}$ and $\nu=\frac{c}{d}$ are substituted into Eq. (9). In Fig. 3, the resulting PDFs can be seen in superposition with the distributions obtained from the numerical simulations. The replication distribution [Eq. (9)] yields a close approximation of the numerical result.

IV. DISCUSSION

At low values of the CO partial pressure, the KEE model remains close to the onset of periodic behavior (Hopf bifurcation) and oscillations are approximately harmonic. Consequently, we find agreement with the CGLE [6]. In particular, we observe constant creation and quadratic annihilation rates and a squared Poisson distribution for the number of defects in the system, see Figs. 3(a), 4(a), and 4(d). With increasing

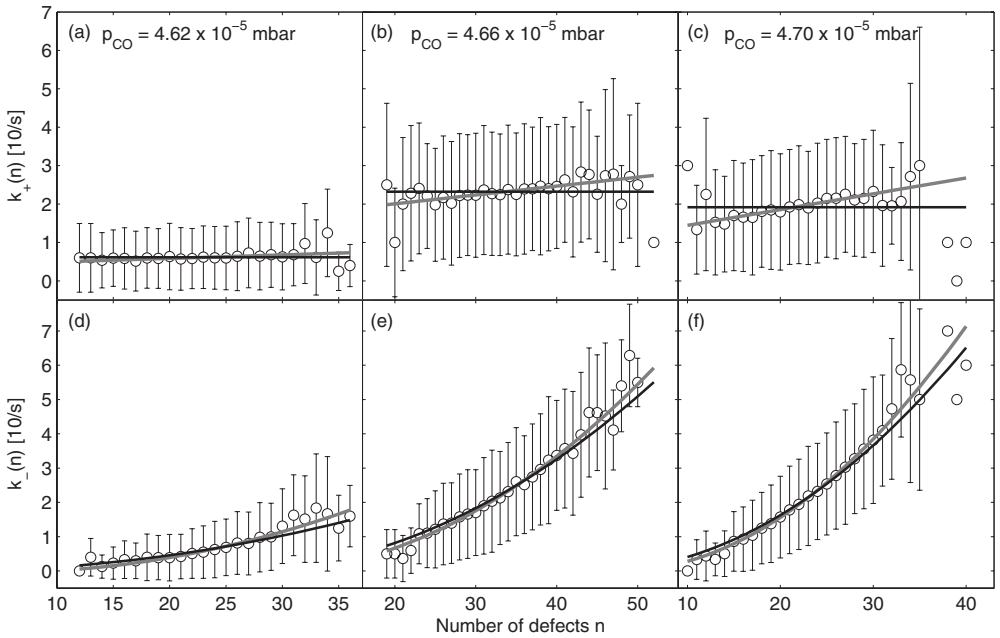

FIG. 4. Defect gain and loss rates, [(a)–(c)] creation, and [(d)–(f)] annihilation rates. Open circles show the rates obtained from numerical simulations of the KEE model for different values of the CO partial pressure, [(a) and (d)] $p_{CO}=4.62\times10^{-5}$ mbar, [(b) and (e)] 4.66×10^{-5} mbar, and [(c) and (f)] 4.70×10^{-5} mbar, respectively. The other model parameters are as listed in Table I. The black lines show constant fits $k_+=c$ in (a)–(c) and square fits $k_-=an^2$ in (d)–(f). The gray lines display linear fits $k_+=c+dn$ in (a)–(c) and combined square and linear fits $k_-=an^2+bn$ in (d)–(f).

CO partial pressure, i.e., with increasing distance from the Hopf bifurcation, oscillations become anharmonic and the dynamics of the KEE model can no longer be approximated by the CGLE. Here, we find a linear dependence of the creation rate on n. In this regime, defects replicate, i.e., defect creation is enhanced when defects are already present in the system [36]. This autocatalytic contribution to defect creation becomes stronger for increasing p_{CO}, see Fig. 4. The resulting PDF shows deviations from a squared Poisson distribution and can be captured by the replication distribution according to Eq. (9), see Figs. 3(b) and 3(c). Defect replication has already been observed in earlier work on the KEE model under global delayed feedback [35]. Note that a linear creation rate was also reported for defect-mediated turbulence in the BZ reaction [37]. It remains an open question to elucidate the mechanism that relates the anharmonicity of oscillations to autocatalytic defect creation.

Let us now compare the numerical results for the KEE model with the analysis of experimental data from catalytic CO oxidation that was reported in Ref. [30]. For the experimental data, the linear dependence of the creation rate on n has not been observed. We thus conclude, that the experiments were conducted in a regime that corresponds to the low-pressure situation of the KEE model [note that agreement between experiments of catalytic CO oxidation on Pt(110) and the KEE model are known to be qualitative, see, e.g., Refs. [25,35]]. For the annihilation rate, the experimental data has shown a combined linear and quadratic annihilation rate. The linear contribution in the annihilation has been explained by the presence of strong short-range correlations between defects of opposite topological charge. These correlations reflect that a large number of defect pairs self-annihilate shortly after creation. The self-annihilating defects cannot be considered as statistically independent well-mixed objects and therefore contribute linearly to the annihilation rate, for a further discussion see Ref. [30]. For the annihilation rate derived from our numerical data we observe only minor differences between the quadratic fit and the combined quadratic and linear fit, see Fig. 4. In fact, it can be seen in Fig. 3 that a modified Poisson distribution does not improve the fit of the numerical histogram. This indicates that self-annihilation events influence defect dynamics to a lesser extent in the model than in the experimental system.

To quantify the influence of self-annihilation events in the model, we have split the total number of defects in our numerical data into two subpopulations separating those defects that self-annihilate from those that annihilate with different partner defects. In Fig. 5, the fraction of self-annihilating defects is shown as a function of CO partial pressure. Although the self-annihilating defects represent about 50% of the total number of defects over time (see the solid curve in Fig. 5), they only account for approximately 15% of the defects at one given instant in time (see the dashed curve in Fig. 5). This is due to the fact that the self-annihilating defects exhibit a much shorter life time than defects that mix and do not self-annihilate. We have also determined separate decay rates for the self-annihilating defects and for defects that annihilate with a different partner defect. As expected, we found a linear decay rate for the self-annihilating subpopulation (data not shown). However, the majority of the defects (85% of the defects that do not self-annihilate) show quadratic annihilation. They dominate the statistics of the total population. In contrast to the experimental results reported in Ref. [30], the decay rate of the total defect popu-

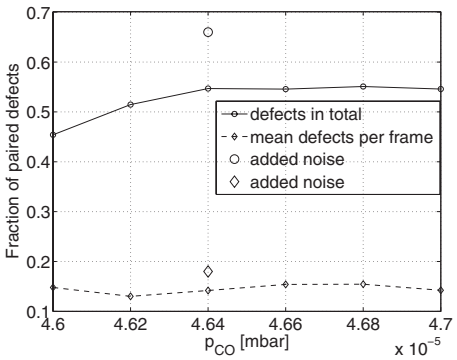

FIG. 5. Fraction of self-annihilating defect pairs as a function of CO partial pressure. The fraction with respect to the total number of defects over time (solid line) and the average fraction at one instant in time (dashed line) is shown. For the model parameters see Table I.

lation in the model is well approximated by a quadratic dependence on n, i.e., self-annihilation events are less important here.

What is the reason for this discrepancy? A fundamental difference between the numerical and the experimental data is the presence of noise in the experimentally recorded images. The influence of noise on the statistics of topological defects has already been investigated in the context of the CGLE [9]. Here, it has been reported that under the influence of noise, defect annihilation follows a combined linear and quadratic dependence on n in contrast to the CGLE without noise, where annihilation is purely quadratic [5]. We thus conjecture that the different decay rates that were observed in experiments with catalytic CO oxidation and in numerical simulations of the KEE model can be attributed to the presence of noise in the experimental data. To support this explanation, we have performed numerical simulations of the KEE model with noise. The noise was implemented such that the local CO coverage was subject to random fluctuations, $\partial_t u = k_1 s_{\mathrm{CO}} p_{\mathrm{CO}}(1-u^3) - k_2 u - k_3 u v + D\nabla^2 u + \sqrt{2}\eta$, where η denotes delta-correlated Gaussian white noise. We chose $p_{\mathrm{CO}} = 4.64 \times 10^{-5}$ mbar and all other parameters as listed in Table I. Again, we determined the subpopulation of defects that self-annihilate. The result is displayed in Fig. 5 by large open symbols. It can be clearly seen that under the influence of noise, more defects undergo self-annihilation. Consequently, the enhanced linear contribution to the decay rate in the experimental data may be due to the presence of noise.

APPENDIX: REPLICATION DISTRIBUTION OF TOPOLOGICAL DEFECTS

In the following, the replication distribution function of the number of topological defects is derived, see also Ref. [38]. Based on the gain and loss rates of defects, $k_+(n)$ and $k_-(n)$, the master equation for the probability $p(n,t)$ reads as

$$\partial_t p(n,t) = k_+(n-1)p(n-1,t) + k_-(n+1)p(n+1,t) - k_+(n)p(n,t) - k_-(n)p(n,t), \tag{A1}$$

where n is the number of defect pairs. In the statistically stationary regime, $\partial_t p(n,t)=0$, Eq. (A1) transforms into a recursive relation for the probability $p(n)$,

$$p(n) = \frac{k_+(n-1)}{k_-(n)} p(n-1). \tag{A2}$$

Based on the rate constants observed in the numerical simulations in Sec. III, the gain and loss rates are approximated by the following expressions:

$$k_+(n) = c + dn, \tag{A3}$$

$$k_-(n) = an^2, \tag{A4}$$

where c denotes a constant contribution to the rate of creation, dn takes defect replication into account, and an^2 is the rate of annihilation. Inserting Eqs. (A3) and (A4) into the recursion relation (A2) yields

$$p(n) = \frac{c + d(n-1)}{an^2} p(n-1) \tag{A5}$$

and can be expanded further to

$$p(n) = p(0) \prod_{k=1}^{n} \frac{c + d(k-1)}{ak^2} = \frac{p(0)}{(n!)^2} \frac{d^n}{a^n} \prod_{k=0}^{n-1} \left(\frac{c}{d} + k \right). \tag{A6}$$

Using the general relation

$$\prod_{k=0}^{n-1} (x+k) = \frac{\Gamma(x+n)}{\Gamma(x)} \equiv (x)_n, \tag{A7}$$

Eq. (A6) can be simplified to

$$p(n) = p(0) \frac{\gamma^n}{(n!)^2} (\nu)_n = p(0) \frac{\gamma^n}{(n!)^2} \frac{\Gamma(\nu+n)}{\Gamma(\nu)}, \tag{A8}$$

with $\gamma = \frac{d}{a}$ and $\nu = \frac{c}{d}$. Since $p(n)$ is a probability, normalization is required,

$$\sum_{n=0}^{\infty} p(n) = 1. \tag{A9}$$

Substituting $p(n)$ from Eq. (A8) into Eq. (A9) leads to

$$p(0) \sum_{n=0}^{\infty} \frac{\gamma^n}{(n!)^2} (\nu)_n = p(0) \sum_{n=0}^{\infty} \frac{\gamma^n}{n!} \frac{(\nu)_n}{(1)_n} = 1, \tag{A10}$$

and thus

$$p(0) = \frac{1}{\Phi(\nu, 1; \gamma)}, \tag{A11}$$

where Φ denotes the degenerate hypergeometric function defined [39]

$$\Phi(\alpha,\beta;z) = 1 + \frac{\alpha}{\beta}z + \frac{\alpha(\alpha+1)}{\beta(\beta+1)}\frac{z^2}{2!} + \cdots = \sum_{n=0}^{\infty}\frac{(\alpha)_n}{(\beta)_n}\frac{z^n}{n!}. \tag{A12}$$

Taking normalization into account, the so-called replication distribution finally reads as

$$p(n) = Q\frac{\gamma^n\Gamma(\nu+n)}{(n!)^2} \quad \text{with} \quad Q = \frac{1}{\Phi(\nu,1;\gamma)\Gamma(\nu)}. \tag{A13}$$

[1] M. C. Cross and P. C. Hohenberg, Rev. Mod. Phys. **65**, 851 (1993).
[2] A. S. Mikhailov, *Foundations of Synergetics I: Distributed Active Systems* (Springer, Berlin, 1994).
[3] E. Ben-Jacob, I. Cohen, and H. Levine, Adv. Phys. **49**, 395 (2000).
[4] S. H. Strogatz, *Nonlinear Dynamics and Chaos* (Perseus, Cambridge, Massachusetts, 1994).
[5] P. Coullet, L. Gil, and J. Lega, Phys. Rev. Lett. **62**, 1619 (1989).
[6] L. Gil, J. Lega, and J. L. Meunier, Phys. Rev. A **41**, 1138 (1990).
[7] H. Chaté and P. Manneville, Physica A **224**, 348 (1996).
[8] M. Hildebrand, M. Bär, and M. Eiswirth, Phys. Rev. Lett. **75**, 1503 (1995).
[9] H. L. Wang, Phys. Rev. Lett. **93**, 154101 (2004).
[10] H. L. Wang and O. Y. Qi, Chaos **15**, 023702 (2005).
[11] J. Davidsen and R. Kapral, Phys. Rev. Lett. **91**, 058303 (2003).
[12] J. Davidsen, M. Zhan, and R. Kapral, Phys. Rev. Lett. **101**, 208302 (2008).
[13] I. Rehberg, S. Rasenat, and V. Steinberg, Phys. Rev. Lett. **62**, 756 (1989).
[14] S. W. Morris, E. Bodenschatz, D. S. Cannell, and G. Ahlers, Phys. Rev. Lett. **71**, 2026 (1993).
[15] K. E. Daniels and E. Bodenschatz, Phys. Rev. Lett. **88**, 034501 (2002).
[16] H. Varela, C. Beta, A. Bonnefont, and K. Krischer, Phys. Rev. Lett. **94**, 174104 (2005).
[17] Q. Ouyang and J.-M. Flesselles, Nature (London) **379**, 143 (1996).
[18] A. S. Mikhailov and K. Showalter, Phys. Rep. **425**, 79 (2006).
[19] R. Imbihl and G. Ertl, Chem. Rev. **95**, 697 (1995).
[20] M. Kim, M. Bertram, M. Pollmann, A. v. Oertzen, A. S. Mikhailov, H. H. Rotermund, and G. Ertl, Science **292**, 1357 (2001).
[21] C. Beta, M. Bertram, A. S. Mikhailov, H. H. Rotermund, and G. Ertl, Phys. Rev. E **67**, 046224 (2003).
[22] M. Stich, C. Punckt, C. Beta, and H. H. Rotermund, Philos. Trans. R. Soc. London, Ser. A **366**, 419 (2008).
[23] M. Bertram, C. Beta, H. H. Rotermund, and G. Ertl, J. Phys. Chem. B **107**, 9610 (2003).
[24] P. S. Bodega, P. Kaira, C. Beta, D. Krefting, D. Bauer, B. Mirwald-Schulz, C. Punckt, and H. H. Rotermund, New J. Phys. **9**, 61 (2007).
[25] M. Bertram, C. Beta, M. Pollmann, A. S. Mikhailov, H. H. Rotermund, and G. Ertl, Phys. Rev. E **67**, 036208 (2003).
[26] C. Beta, M. G. Moula, A. S. Mikhailov, H. H. Rotermund, and G. Ertl, Phys. Rev. Lett. **93**, 188302 (2004).
[27] J. Wolff, A. G. Papathanasiou, I. G. Kevrekidis, H. H. Rotermund, and G. Ertl, Science **294**, 134 (2001).
[28] J. Wolff, M. Stich, C. Beta, and H. H. Rotermund, J. Phys. Chem. B **108**, 14282 (2004).
[29] S. Jakubith, H. H. Rotermund, W. Engel, A. von Oertzen, and G. Ertl, Phys. Rev. Lett. **65**, 3013 (1990).
[30] C. Beta, A. S. Mikhailov, H. H. Rotermund, and G. Ertl, Europhys. Lett. **75**, 868 (2006).
[31] K. Krischer, M. Eiswirth, and G. Ertl, J. Chem. Phys. **96**, 9161 (1992).
[32] J. Davidsen, A. Mikhailov, and R. Kapral, Phys. Rev. E **72**, 046214 (2005).
[33] C. Punckt, M. Stich, C. Beta, and H. H. Rotermund, Phys. Rev. E **77**, 046222 (2008).
[34] M. Bertram and A. S. Mikhailov, Phys. Rev. E **63**, 066102 (2001).
[35] M. Bertram and A. S. Mikhailov, Phys. Rev. E **67**, 036207 (2003).
[36] A. S. Mikhailov and A. Y. Loskutov, *Foundations of Synergetics II* (Springer, Berlin, 1996).
[37] C. Qiao, H. Wang, and Q. Ouyang, Phys. Rev. E **79**, 016212 (2009).
[38] C. Beta, Ph.D thesis, Freie Universität Berlin, 2004.
[39] I. S. Gradshteyn and I. M. Ryzhik, in *Table of Integrals, Series, and Products*, edited by A. Jeffrey (Academic, New York, 1965).